White Rose Research Online

eprints@whiterose.ac.uk
https://eprints.whiterose.ac.uk
Universities of Leeds, Sheffield and York

Deposited via The University of Sheffield.

White Rose Research Online URL for this paper:
https://eprints.whiterose.ac.uk/id/eprint/248143/

Version: Accepted Version

**Article:**
Hammond, J., Thornton, J. and Brown, S. (2027) Beyond Euclidean distance: The impact of flow-dependent economics on CCS network design. Computers & Chemical Engineering, 216. 109912. ISSN: 0098-1354

https://doi.org/10.1016/j.compchemeng.2026.109912

© 2026 The Authors. Except as otherwise noted, this author-accepted version of a journal article published in Computers & Chemical Engineering is made available via the University of Sheffield Research Publications and Copyright Policy under the terms of the Creative Commons Attribution 4.0 International License (CC-BY 4.0), which permits unrestricted use, distribution and reproduction in any medium, provided the original work is properly cited. To view a copy of this licence, visit http://creativecommons.org/licenses/by/4.0/

**Reuse**
This article is distributed under the terms of the Creative Commons Attribution (CC BY) licence. This licence allows you to distribute, remix, tweak, and build upon the work, even commercially, as long as you credit the authors for the original work. More information and the full terms of the licence here: https://creativecommons.org/licenses/

**Takedown**
If you consider content in White Rose Research Online to be in breach of UK law, please notify us by emailing eprints@whiterose.ac.uk including the URL of the record and the reason for the withdrawal request.

UNIVERSITY OF LEEDS
University of Sheffield
UNIVERSITY of York

# Beyond Euclidean Distance: The Impact of Flow-Dependent Economics on CCS Network Design

Joseph Hammond[a], Joel Thornton[a], Solomon Brown[a,*]

[a]*School of Chemical, Materials & Biological Engineering, The University of Sheffield, Mappin Street, Sheffield, S1 3JD, UK*

**Abstract**

Many CCS transport studies determine pipeline corridors using minimum-length or cost-surface heuristics and then size pipelines on the resulting fixed layout. This decomposition is computationally attractive, but it neglects flow-dependent pipeline economics: the network's topology determines how flows concentrate on shared segments, which shifts pipeline diameter choices and can materially change total cost. We develop a two-stage framework that internalises flow-dependence in routing while retaining tractability at cluster scale. A raster-penalty genetic algorithm first generates tree topologies under either a minimum-length or a flow-dependent surrogate objective ($L_{ij}^{w}\,|Q_{ij}|^{b}$); each topology is then sized and costed using the same hydraulic model with discrete commercial diameters. Applied to the Humber industrial region (UK), the flow-dependent routing objective produces networks with greater spatial overlap with the published onshore CCS corridor than the penalty-weighted-length heuristic, while an illustrative peripheral-intensification case shows that backbone placement responds to changes in flow distribution. In the full regional build-out case, the best-found layouts generated by the flow-aware surrogate are approximately 6% longer in geometric length but have approximately 35% lower estimated CAPEX than layouts generated by the otherwise identical penalty-weighted-length routing heuristic when both are evaluated using the same Stage 2 model. The results show that, relative to penalty-weighted-length routing within the adopted framework, internalising flow dependence in Stage 1 can materially affect trunk placement and reduce estimated pipeline CAPEX.

*Keywords:* CCS, pipeline routing, $CO_2$ transport, Spatial optimisation, Genetic algorithm

*Corresponding author.
*Email address:* s.f.brown@sheffield.ac.uk (Solomon Brown)

**Nomenclature and Terminology**

**Acronyms**

AONB Area of Outstanding Natural Beauty

CAPEX Capital expenditure

CCS Carbon capture and storage

CEPCI Chemical Engineering Plant Cost Index

CRoW Countryside and Rights of Way (access land)

DN Nominal diameter

GA Genetic algorithm

GIS Geographic information system

HCCP Humber Carbon Capture Pipeline

MOP Maximum operating pressure

MST Minimum spanning tree

NAEI National Atmospheric Emissions Inventory

OPEX Operating expenditure

ROW Right-of-way

SAC Special Area of Conservation

SMYS Specified minimum yield stress

SPA Special Protection Area

SSSI Site of Special Scientific Interest

StObGA Steiner tree with Obstacles Genetic Algorithm

UK United Kingdom

US United States

**Symbols**

| | |
|---|---|
| $(x_\ell, y_\ell)$ | Coordinates of movable (Steiner / bifurcation) node $\ell$ (m) |
| $\bar{\phi}^{\text{net}}$ | Mean penalty multiplier of a network, $\sum L^w / \sum L$ (–) |
| $\bar{\phi}_{ij}$ | Mean penalty multiplier on arc $(i, j)$, $\bar{\phi}_{ij} = L^w_{ij}/L_{ij}$ (–) |
| $\Delta P_{ij}$ | Pressure drop on arc $(i, j)$, $P_i - P_j$ (Pa) |
| $\dot{V}^p_{ij}$ | Per-pipeline volumetric flow on arc $(i, j)$ ($m^3$/s) |
| $\dot{V}_{ij}$ | Total volumetric flow on arc $(i, j)$ ($m^3$/s) |
| $\ell_{ij}(g)$ | Length of arc $(i, j)$ lying within raster cell $g$ (km) |
| $\kappa^{DF}$ | Design factor (–) |
| $\kappa^E$ | Longitudinal joint factor (–) |
| $\mathbb{I}_{fg}$ | Indicator: 1 if cell $g$ is covered by feature $f$, else 0 (–) |
| $\mathbf{b}$ | Binary waypoint-activation vector (–) |
| $\mathcal{D}$ | Set of commercial diameter–schedule options (–) |
| $\mathcal{F}$ | Set of penalty feature layers (–) |
| $\mathcal{G}$ | Set of raster cells (–) |
| $\mathcal{S}_j$ | Node set in subtree rooted at $j$ when arc $(i, j)$ is removed (–) |
| $\mu$ | Dynamic viscosity (Pa·s) |
| $\phi_g$ | Raster cell penalty multiplier (–) |
| $\rho$ | Assumed $CO_2$ density ($kg/m^3$) |
| $\tau^w$ | Allowable wall shear stress (Pa) |
| $\tau^p$ | Specified minimum yield stress (SMYS) (Pa) |
| $\xi$ | Pipe absolute roughness (m) |
| $A$ | Set of arcs / segments (–) |

$b$ Flow-cost exponent in surrogate objective (–)

$B_{ijd}$ Binary selection of catalogue option $d$ for arc $(i, j)$ (–)

$C$ Total network objective cost in Stage 2 (currency units as stated)

$C_{ij}^{C}$ Segment capital cost (CAPEX) for arc $(i, j)$ (£ thousand)

$d$ Diameter–schedule option index (–)

$D_{d}^{pi}$ Catalogue inner diameter for option $d$ (m)

$D_{ij}^{pi}$ Selected inner diameter on arc $(i, j)$ (m)

$D_{ij}^{po,in}$ Selected outer diameter on arc $(i, j)$ (inches)

$D_{d}^{po}$ Catalogue outer diameter for option $d$ (m)

$D_{ij}^{po}$ Selected outer diameter on arc $(i, j)$ (m)

$f$ Penalty feature layer index (–)

$F(T)$ Generic Stage 1 fitness / objective value for tree $T$ (–)

$F_A(T)$ Model A fitness: minimum penalty-weighted length (km)

$F_B(T)$ Model B fitness: flow-dependent surrogate objective (–)

$f_D$ Darcy friction factor (–)

$g$ Raster cell index (–)

$i, j$ Node indices (–)

$K$ Number of waypoint candidates (length of $\mathbf{b}$) (–)

$k$ Node index for injections/balances (–)

$L_{ij}^{w}$ Penalty-weighted length of arc $(i, j)$ (km)

$L_{ij}$ Geometric length of arc $(i, j)$ (km)

$N$ Set of nodes (–)

$N_{ij}^{p}$ Number of parallel pipelines on arc $(i, j)$ (–)

$P^{\mathrm{MOP}}$ Maximum operating pressure (Pa)

$P^{\max}$ Maximum allowable node pressure (Pa)

$P^{\min}$ Minimum allowable node pressure (Pa)

$P_i$ Pressure at node $i$ (Pa)

$Q_{ij}^{p}$ Per-pipeline mass flow on arc $(i, j)$ (MtCO$_2$/yr)

$q_k$ Net injection at node $k$ (+source, –sink) (MtCO$_2$/yr)

$Q_{ij}$ Design mass flow on arc $(i, j)$ (MtCO$_2$/yr)

$r$ Buffer radius used in route-overlap metric (m)

$s$ Number of movable nodes in the genome (–)

$T = (N, A)$ Tree network with node set $N$ and arc set $A$ (–)

$t_d$ Wall thickness for option $d$ (m)

$t_{ij}$ Selected wall thickness on arc $(i, j)$ (m)

$v^{e}$ Erosion (shear-limited) velocity (m/s)

$v^{\max}$ Maximum allowable velocity (m/s)

$v_{ij}$ CO$_2$ velocity in a pipeline on arc $(i, j)$ (m/s)

$w_f$ Penalty multiplier assigned to feature layer $f$ (–)

## 1. Introduction

Carbon capture and storage (CCS) at scale will require new CO$_2$ transport networks that connect multiple, spatially distributed industrial sources to shared storage sites. Most national and regional CCS infrastructure studies represent these networks using simplified routing and costing assumptions to retain computational tractability [1–3]. Common approaches derive tree topologies from minimum-length spanning networks or from shortest paths over coarse cost surfaces, and then size pipelines as a separate step given fixed routes and assumed flows [4, 5]. These practices implicitly treat transport cost as approximately proportional to distance (sometimes adjusted by spatial penalties) and largely independent of how flows are distributed across the network.

In reality, routing and design are coupled through flow-dependent pipeline economics. The cost per kilometre of a $CO_2$ trunk line depends non-linearly on flow through pipeline diameter, pressure and structural requirements [6, 7]. Changing the layout changes how flow is concentrated on shared segments, which can alter required diameters and materially affect total cost. Classical network design results therefore show that minimum-length trees need not coincide with minimum-cost networks once link costs depend on flow and technology choices [8, 9]. André et al. couple topology modification with pipeline sizing and demonstrate cost reductions relative to a minimum spanning tree [10]; Heijnen et al. develop a minimum-cost Gilbert-tree method under generic flow-dependent cost functions [9]; and Yeates et al. compare graph-based heuristics for minimum-cost $CO_2$ capacitated trees using a concave flow-cost relationship [11]. These studies establish the importance of flow-dependent topology design, but formulate the problem primarily in Euclidean or fixed-terminal graph settings without heterogeneous geographical costs during corridor generation.

A parallel strand of infrastructure-planning research introduces geography through least-cost paths, spatial cost surfaces or pre-generated candidate networks [4, 5, 12]. Our previous work extended this approach by using the Steiner tree with Obstacles Genetic Algorithm (StObGA) to search network topology and corridor geometry over a heterogeneous geographical penalty surface, followed by detailed pipeline sizing [13]. However, routing remained governed by penalty-weighted length, with flow-dependent engineering costs introduced only after the route and topology had been determined. This leaves an important methodological gap between flow-aware minimum-cost tree design and geography-constrained pipeline routing: flow concentration should influence the placement of shared corridors during route generation, rather than only their subsequent sizing.

This paper therefore asks: how does CCS network topology change when flow-dependent transport economics are internalised in geography-constrained routing, and how different are the resulting layouts and costs from those obtained through penalty-weighted-length routing? We use a two-stage framework. In Stage 1, a penalty-surface genetic algorithm designs tree topologies under either (i) a penalty-weighted-length objective or (ii) a flow-dependent surrogate objective of the form $\sum L_{ij}^{w}|Q_{ij}|^{b}$, building on the minimum-cost tree perspective developed in [9]. In Stage 2, every resulting layout is evaluated using the same detailed pipeline sizing and costing model, isolating the effect of the Stage 1 routing objective on system-level outcomes.

The paper makes three contributions. First, it embeds a concave flow-capacity surrogate within StObGA, extending geography-constrained route generation from penalty-weighted-length to flow-aware routing. Second, it provides a controlled comparison in which layouts generated under both objectives are evaluated using the same $CO_2$-specific hydraulic, commercial-diameter and pipeline-CAPEX model. Third, it applies the framework to the Humber region, quantifying the resulting differences in trunk placement, network structure and estimated CAPEX, and comparing the

generated layouts with the published HCCP corridor. Together, these contributions connect flow-dependent minimum-cost tree design with spatially explicit CCS corridor generation and detailed engineering evaluation.

We apply the framework to a UK CCS case study in the Humber region and evaluate three scenarios: (i) a corridor-comparison case representing the currently developed network, (ii) a full regional build-out connecting all major emitters, and (iii) an illustrative stress test in which a peripheral site's emission is increased to examine backbone responsiveness. In the full build-out case, the best-found flow-aware layouts are approximately 6% longer in geometric length but have approximately 35% lower estimated CAPEX than layouts generated by the otherwise identical penalty-weighted-length routing heuristic. Within the adopted case-study assumptions, the results demonstrate that the Stage 1 routing objective can materially affect trunk placement and the costs obtained after detailed pipeline sizing.

The remainder of the paper is organised as follows. Section 2 describes the routing and costing framework. Section 3 introduces the case study and scenarios. Section 4 presents results and discusses implications for CCS network modelling. Section 5 concludes.

## 2. Methodology

We use a two-stage framework to isolate how the routing objective influences CCS network topology and cost. In Stage 1, a penalty-surface genetic algorithm (GA) generates candidate tree topologies over a continuous spatial domain, but evaluates corridor desirability using a shared raster penalty surface. Two GA variants are compared: Model A minimises penalty-weighted network length, while Model B minimises a flow-dependent surrogate objective of the form $\sum L_{ij}^{w}|Q_{ij}|^{b}$. In Stage 2, every Stage 1 topology is evaluated using the same pipeline sizing and costing optimisation model. Because Stage 2 is identical for both routing variants, differences in final cost and diameter allocation can be attributed to the Stage 1 objective rather than to inconsistent design assumptions.

### *2.1. Stage 1: routing and topology optimisation on a raster penalty surface*

#### *2.1.1. Penalty-weighted segment length*

Let $\mathcal{G}$ be the set of raster cells covering the study area. Each cell $g \in \mathcal{G}$ is assigned a penalty multiplier $\phi_g \geq 1$ derived from spatial constraint layers (Section 3). The cell multiplier is constructed by additively combining overlapping GIS layers in excess over baseline:

$$\phi_g \;=\; 1 + \sum_{f \in \mathcal{F}} (w_f - 1)\, \mathbb{I}_{fg}, \tag{1}$$

where $\mathcal{F}$ is the set of feature layers, $w_f \geq 1$ is the layer-specific multiplier (Appendix B), and $\mathbb{I}_{fg} \in \{0, 1\}$ indicates whether cell $g$ is covered by feature $f$.

A decoded network is a tree $T = (N, A)$ with arc set $A$. Each arc $(i, j) \in A$ is published as a straight-line segment in continuous space, and its penalty-weighted length is evaluated against the raster as

$$L_{ij}^{w} = \sum_{g \in \mathcal{G}} \phi_g \, \ell_{ij}(g), \tag{2}$$

where $\ell_{ij}(g)$ is the length of segment $(i, j)$ lying within cell $g$. By construction, $\phi_g = 1$ denotes unconstrained terrain, so $L_{ij}^{w} = L_{ij}$ when no penalised cells are traversed. The corresponding geometric length is $L_{ij} = \sum_{g \in \mathcal{G}} \ell_{ij}(g)$.

For network-level calculation, we define the mean geospatial penalty factor as the length-weighted average cell multiplier across all arcs:

$$\bar{\phi}^{\text{net}} = \frac{\sum_{(i,j) \in A} L_{ij}^{w}}{\sum_{(i,j) \in A} L_{ij}}, \tag{3}$$

which equals 1 on unconstrained terrain and increases with penalty exposure.

*2.1.2. Genome encoding and decoding to a feasible tree*

Candidate networks are generated using the Steiner tree with Obstacles Genetic Algorithm (StObGA) [14], following the implementation approach in [13]. Each candidate is encoded by a genome comprising (i) coordinates of movable nodes (Steiner and bifurcation nodes) and (ii) a fixed-length binary vector that activates a subset of waypoint candidates:

$$\Big\{(x_1, y_1), \ldots, (x_s, y_s)\Big\} \parallel \mathbf{b}, \qquad \mathbf{b} \in \{0, 1\}^K. \tag{4}$$

Terminal nodes are fixed and always included. Activated waypoints provide candidate bend/junction locations that help represent plausible detours and corridor-following behaviour on the raster surface with a compact encoding.

Decoding proceeds by forming a node set comprising terminals, the $s$ movable nodes, and the activated waypoints. A complete graph is constructed on this node set, where each edge is assigned a weight equal to its raster-weighted length computed by Eq. (2). A minimum spanning tree (MST) is then computed on the weighted complete graph (e.g., Prim's algorithm), yielding a loop-free network that connects all terminals. Genetic search (selection, crossover, mutation, and feasibility repair) follows [13, 14]; GA parameters are reported in Appendix A.

The MST decoder provides a feasible tree for every genome, consistent with the restriction to connected, loop-free networks. The node set supplied to the decoder is not limited to the fixed terminals: each genome also specifies the locations of movable nodes and the waypoints that are activated. Consequently, both the connections between nodes and the resulting corridor geometry can vary across genomes. Although the decoder favours lower penalty-weighted

connections for a given node set, both models use the same decoder and genetic operators; the comparison therefore isolates the effect of the Stage 1 objective within a common search representation.

#### *2.1.3. Flow assignment on a tree*

For a decoded tree, flows are assigned by nodal balance. Let $q_k$ denote the net injection at node $k \in N$ (positive for $CO_2$ sources, negative for sinks), expressed in $MtCO_2/yr$, with $\sum_{k \in N} q_k = 0$. Because the network is a tree, the flow on each arc is uniquely determined. Taking the sink as the reference (root) node, the magnitude of flow on arc $(i, j)$ is computed as the absolute net injection in the downstream component:

$$|Q_{ij}| = \left| \sum_{k \in \mathcal{S}_j} q_k \right|, \tag{5}$$

where $\mathcal{S}_j$ is the node set in the subtree rooted at $j$ when arc $(i, j)$ is removed. These arc flows are used in the Stage 1 flow-dependent objective (Model B) and passed to the Stage 2 sizing model.

#### *2.1.4. Stage 1 objectives: Model A vs Model B*

For each decoded tree $T = (N, A)$, the GA assigns a scalar fitness (objective) value $F(T)$ to be minimised. We consider two alternatives: Model A uses a length-based fitness $F_A(T)$, while Model B uses a flow-dependent fitness $F_B(T)$.

Model A (minimum-length) minimises total raster-weighted network length:

$$F_A(T) = \sum_{(i,j) \in A} L_{ij}^{w}, \tag{6}$$

Model B (minimum-cost surrogate) introduces flow-dependent economics using a capacity-cost exponent $b \in (0, 1)$:

$$F_B(T) = \sum_{(i,j) \in A} L_{ij}^{w} \, |Q_{ij}|^{b}, \tag{7}$$

This surrogate captures economies of scale in transport: concentrating flow on shared segments can reduce unit cost, but may change topology and routing. We specify $b = 0.6$ a priori as the baseline, consistent with its established use as an approximation of $CO_2$ pipeline capacity-cost relationships [9]. Section 4 additionally illustrates the directional effect of lower and higher exponent values.

### 2.2. *Stage 2: pipeline sizing and cost evaluation*

Each Stage 1 tree is evaluated using a common pipeline sizing and costing optimisation model based on [7]. For a given topology $T = (N, A)$, each arc $(i, j) \in A$ is treated as a pipeline segment with geometric length $L_{ij}$ and design flow $Q_{ij}$. The model selects (i) the number of parallel pipelines $N_{ij}^{p}$ and (ii) a diameter option from a discrete commercial catalogue, and determines operating pressures such that hydraulic, structural, and operational constraints are satisfied (e.g., pressure and velocity limits, wall thickness and stress constraints). Full constraint equations and parameter values are provided in Appendix C.

The objective minimises total cost, expressed as capital expenditure (CAPEX):

$$\min \sum_{(i,j)\in A} C_{ij}^{C}. \tag{8}$$

To translate the raster penalty surface into a route-dependent construction uplift, we define the mean penalty factor for arc $(i, j)$ as

$$\bar{\phi}_{ij} \;=\; \frac{L_{ij}^{w}}{L_{ij}} \;=\; \frac{\sum_{g\in\mathcal{G}} \phi_g \, \ell_{ij}(g)}{\sum_{g\in\mathcal{G}} \ell_{ij}(g)}, \qquad \bar{\phi}_{ij} \geq 1, \tag{9}$$

where $L_{ij}^{w}$ is the raster-weighted length from Eq. (2), and $L_{ij} = \sum_{g\in\mathcal{G}} \ell_{ij}(g)$ is the geometric length of the segment.

Segment CAPEX is then computed by applying $\bar{\phi}_{ij}$ as a multiplicative uplift to the $CO_2$ pipeline cost correlations of McCoy and Rubin [15]:

$$\begin{aligned} C_{ij}^{C} \;=\; N_{ij}^{p}\, \bar{\phi}_{ij} \Big[ & 6.516 \left(D_{ij}^{po,in}\right)^{1.59} L_{ij}^{0.901} + 28.9 \left(D_{ij}^{po,in}\right)^{0.94} L_{ij}^{0.82} \\ & + 16.32 \left(D_{ij}^{po,in}\right)^{0.403} L_{ij}^{1.049} + 33.13 \left(D_{ij}^{po,in}\right)^{0.791} L_{ij}^{0.783} \Big], \end{aligned} \tag{10}$$

where $D_{ij}$ is the selected pipeline outside diameter from a discrete catalogue for arc $(i, j)$, and the four terms correspond to materials, labour, ROW and miscellaneous costs, respectively [15]. $D_{ij}^{po,in}$ is in inches and $L_{ij}$ in km, yielding $C_{ij}^{C}$ in £ thousand, 2025 GBP. The coefficients in Eq. (10) are expressed on the study cost basis (May 2025 GBP, including CEPCI escalation, currency conversion, and UK uplift assumptions; Appendix D). Details of the diameter catalogue are given in Section 3.

Importantly, the same Stage 2 model, cost correlations, and constraints are applied to layouts from both Model A and Model B. Differences in cost and sizing outcomes therefore reflect the impact of the Stage 1 routing objective on topology and flow allocation.

## 3. Case study

We apply the framework to the Humber industrial region in the UK, which contains a dense set of major point-source $CO_2$ emitters and a proposed shared transport corridor to offshore storage—the Humber Carbon Capture Pipeline (HCCP) (Figure 1) [16]. $CO_2$ sources are represented as fixed terminal nodes with specified capture flows, taken from the UK National Atmospheric Emissions Inventory (NAEI) point-source dataset [17]. Storage is represented as a single sink terminal node—Easington terminal. All spatial processing is performed in a projected coordinate system appropriate for UK infrastructure analysis (British National Grid).

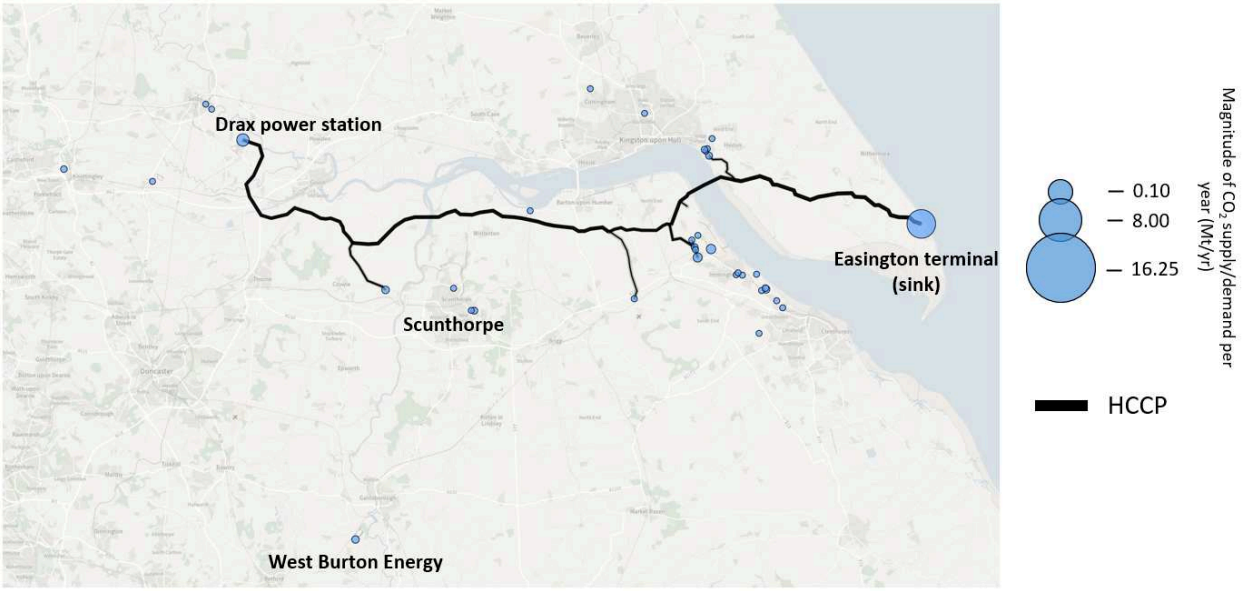



Figure 1: Humber case study: $CO_2$ point sources (circles, sized by annual captured $CO_2$ flow in $MtCO_2/yr$) and the published HCCP onshore $CO_2$ transport corridor (black). Easington terminal is modelled as the single sink, with key locations labelled for reference (Drax, Scunthorpe, West Burton).

The GIS feature layers include case study-relevant geographical constraints such as environmentally sensitive areas, cultural heritage designations, land-use constraints, and major linear features relevant to routing. Feature weights and data sources used to construct $\phi_g$ are specified *ex ante* and reported in Appendix B; they are not tuned to match the engineered corridor used in Scenario 1.

For Scenarios 1–2, each routing model is replicated across multiple GA runs using distinct random seeds to quantify stochastic variability; Scenario 3 is run once as an illustrative stress test (Section 4).

All candidate trees from Stage 1 are evaluated using the same Stage 2 sizing and costing optimisation model (Section 2). Pipeline diameters are selected from a discrete commercial catalogue comprising 817 unique inner/outer diameter pairs spanning DN6 to DN2300 across a wide range of schedules. Segment CAPEX is computed using the McCoy and Rubin $CO_2$ pipeline cost correlations [15] expressed on the study cost basis (2025 GBP; Appendix D)

and uplifted by the route-dependent mean penalty factor $\bar{\phi}_{ij}$ (Eq. (10)). Hydraulic, structural, and operational constraints (including pressure and velocity limits and wall-thickness/stress constraints) follow [7] and are reported in Appendix C.

Three scenarios are used to test (i) alignment with an engineered corridor, (ii) topology and cost differences at full regional build-out, and (iii) sensitivity of the backbone to spatial redistribution of flow:

1. **Scenario 1 (comparison)** includes six major emitters consistent with the currently developed Humber transport corridor; modelled routes are compared to the published engineered trunk alignment using a buffer-overlap metric (Section 4).

2. **Scenario 2 (full build-out)** connects all identified major emitters in the region (35 sources), allowing trunk-and-branch structure to emerge endogenously.

3. **Scenario 3 (peripheral intensification)** modifies Scenario 2 by increasing capture at a peripheral source to test how strongly a single large emitter pulls the economically optimal trunk; the minimum-length model is unchanged under this perturbation because it depends only on terminal locations and penalties.

## 4. Results and discussion

This section compares networks produced by the two Stage 1 routing objectives when evaluated under a common Stage 2 sizing and costing model. Model A minimises penalty-weighted length (Eq. 6); Model B minimises a flow-dependent surrogate (Eq. 7) with baseline exponent $b = 0.6$. For Scenarios 1–2, each model is run five times using distinct random seeds, and every resulting topology is sized and costed with identical hydraulic and economic assumptions. Scenario 3 is run once as an illustrative case to examine backbone responsiveness under Model B.

We consider three configurations: (i) the current CCS development plan in the region (Scenario 1), (ii) a fully expanded network connecting all major emitters (Scenario 2), and (iii) a modified case with increased emissions at a peripheral source (Scenario 3). Results are organised around three questions:

**Q1: Comparison:** Does the flow-dependent objective align more closely with the published CCS corridor more closely than a minimum-length design?

**Q2: System design:** In a fully expanded regional network, how different are the resulting topologies, total length, and cost?

**Q3: Spatial sensitivity:** How does the economically optimal backbone respond when emissions are redistributed spatially?

### *4.1. Comparison with the published HCCP corridor (Scenario 1 comparison)*

Scenario 1 mirrors the current CCS development plan in the Humber region. Figure 2 overlays the published HCCP onshore $CO_2$ network (black) with networks obtained from Model A (yellow) and Model B (blue) across five GA runs each. All solutions follow the same broad east–west structure, but the networks differ in their alignment with the engineered corridor. Model B layouts form a tight cluster around the published network, particularly through the constrained central section, whereas Model A layouts exhibit larger deviations and a broader fan of alternatives.

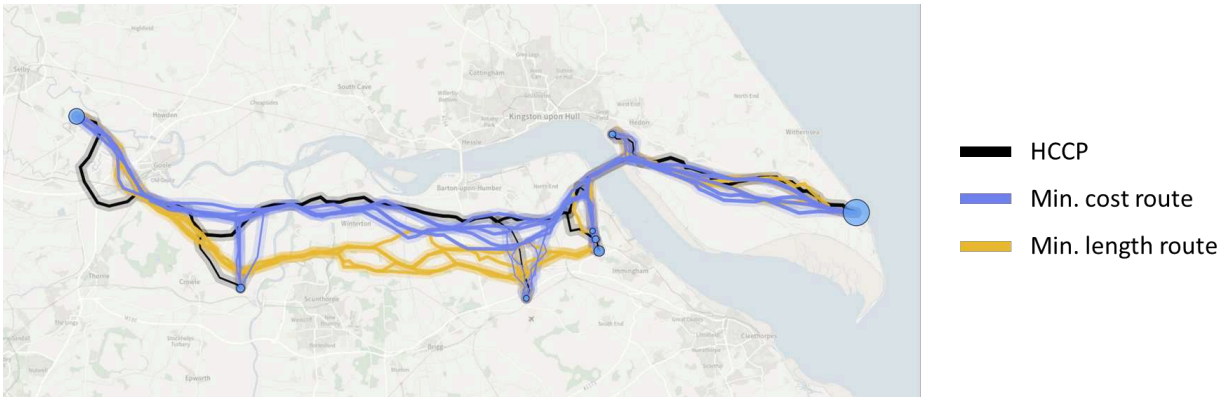



Figure 2: Scenario 1 (comparison): published HCCP onshore network (black) overlaid with five GA solutions from Model A (minimum length; yellow) and Model B (minimum-cost surrogate; blue).

To quantify network similarity, Figure 3 reports the proportion of total modelled network length lying within a buffer of radius $r$ around the published HCCP network, as $r$ increases. Shaded bands show the spread across runs and solid lines show the mean. At any given radius, Model B places a larger fraction of its network within the buffer than Model A. For example, to capture 50% of network length, Model B requires a buffer of $556 \pm 126$ m, compared with $848 \pm 112$ m for Model A. For 75% coverage, the required radii are $1{,}208 \pm 180$ m and $2{,}626 \pm 213$ m, respectively, and for 90% coverage they are $1{,}828 \pm 232$ m versus $4{,}608 \pm 449$ m. Equivalently, Model A requires roughly $1.3$–$2.5\times$ larger buffers to achieve the same overlap with the published corridor.

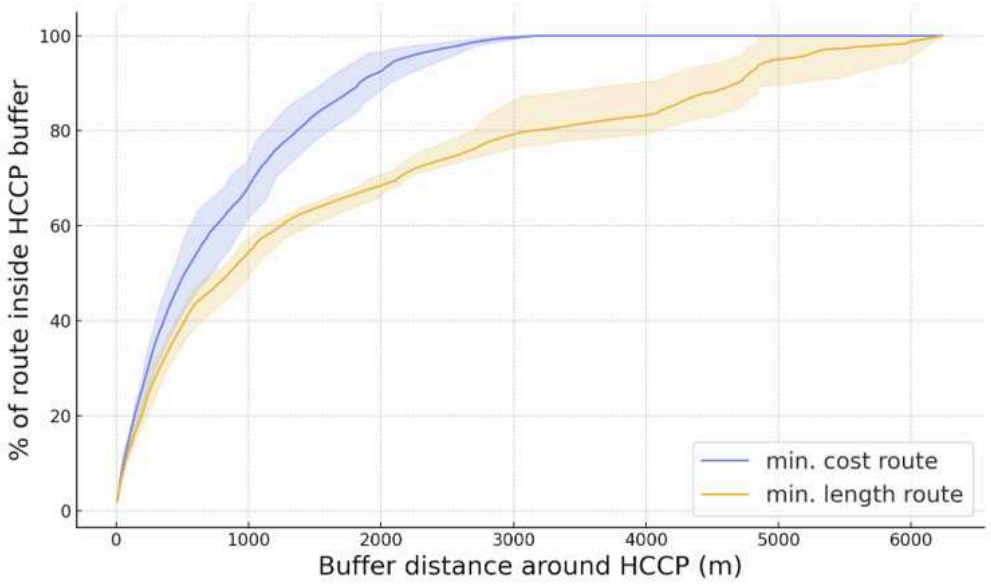



Figure 3: Scenario 1: buffer-overlap metric showing the percentage of total modelled network length within a radius $r$ of the published HCCP network. Lines show the mean across five runs; shaded bands show $\pm 1$ SD.

The ordering is consistent across runs, with limited band overlap over most of the buffer range. In this corridor-comparison case, internalising flow-dependent economics in the routing objective therefore yields network layouts that are closer to the engineered CCS network than those obtained from penalty-weighted length minimisation, despite using no explicit information about the consented alignment.

### *4.2. Full regional CCS network (Scenario 2)*

Scenario 2 represents a full regional CCS build-out in which all identified major emitters are connected to a single sink. Figure 4 compares one representative network from each routing model, selected as the run whose total CAPEX is closest to that model's five-run mean. Table 1 reports mean $\pm$ SD across five independent GA runs per model.

For reporting trunk–branch metrics, we define the trunk as the unique path on the tree between the Easington terminal and the Drax power station. This definition is used purely for reporting because the Easington–Drax corridor corresponds to the dominant onshore backbone in the regional development concept; it is not imposed as a constraint in either routing model. All remaining arcs are classified as branches. Trunk length share is the ratio of trunk geometric length to total geometric network length, and trunk CAPEX share is the ratio of trunk CAPEX to total network CAPEX (both computed after Stage 2 sizing).

The two objectives produce visibly different trunk–branch structures (Figure 4). Model A (minimum-length) prioritises a short penalty-weighted tree and, as an emergent outcome, tends to avoid a direct crossing of the high-penalty Humber estuary corridor. This induces a long, sweeping "C-shaped" design that routes around the constrained

central area and collects many sources with small spurs. In contrast, Model B (minimum-cost surrogate) maintains a comparatively direct east–west backbone, accepting higher-penalty terrain where necessary, and instead expresses more of the connectivity through long spurs. In other words, Model A reduces corridor difficulty at the expense of a longer high-flow backbone, whereas Model B protects the backbone length and absorbs the remaining connectivity via lower-flow branches.




Figure 4: Scenario 2 (full build-out): representative networks from Model A (left) and Model B (right), chosen as the runs with CAPEX closest to the five-run mean for each model.

Table 1 shows that Model B yields networks that are longer in geometric terms but markedly cheaper once sized and costed. Relative to Model A, the geometric length increases from $276.90 \pm 2.77$ km to $294.34 \pm 4.21$ km (a $+6.3\%$ increase). Consistent with the visual interpretation above, Model B also exhibits a higher mean geospatial penalty factor ($1.89 \pm 0.10$ vs. $1.63 \pm 0.03$, a $+16.0\%$ increase), indicating that the cost-based optimisation is willing to traverse more constrained terrain when doing so shortens or reshapes the high-capacity corridors. Combining these two effects, the implied total penalty-weighted exposure (approximated by total length multiplied by the mean penalty factor) is substantially higher under Model B, reinforcing that Model B is not simply minimising the same spatial proxy more effectively.

Table 1: Scenario 2 (full build-out): comparison of network metrics across five GA replications (mean±SD). All candidate layouts are evaluated using the same Stage 2 sizing and costing model.

| **Metric** | **Model A (penalty-weighted length)** | **Model B (flow-aware surrogate)** |
|---|---|---|
| Total geometric length (km) | $276.90 \pm 2.77$ | $294.34 \pm 4.21$ |
| Avg. geospatial penalty factor | $1.63 \pm 0.03$ | $1.89 \pm 0.10$ |
| CAPEX (£M) | $905.92 \pm 8.71$ | $587.36 \pm 6.97$ |
| Cost per length (£M/km) | $3.27 \pm 0.02$ | $2.00 \pm 0.02$ |

Despite this, total CAPEX falls from $905.92 \pm 8.71$ £M (Model A) to $587.36 \pm 6.97$ £M (Model B), a reduction of

approximately $35\%$. Normalising by geometric length, the cost intensity drops from $\approx 3.27$ £M/km to $\approx 2.00$ £M/km (about $39\%$ lower). The standard deviations across runs are small relative to these differences (typically $\sim 1\%$ of the mean for length and CAPEX), indicating that the cost advantage is not an artefact of GA stochasticity.

The key point is that, under flow-dependent economics, the length of the high-flow backbone dominates system CAPEX more than the total network length or average spatial penalty. Model A's objective is insensitive to how flows concentrate on shared corridors, so it can inadvertently create a long trunk that carries aggregated flow over large distances. Model B internalises this incentive (via the $L_{ij}^{w}|Q_{ij}|^{b}$ surrogate), and therefore accepts additional branching and higher-penalty segments to keep the main corridor shorter and to redistribute capacity requirements across more, smaller-flow segments. This explains how Model B can be simultaneously longer and more penalty-exposed in a spatial sense, yet substantially cheaper once evaluated using the same detailed sizing model.

### *4.3. Illustrative effect of the "economies-of-scale" exponent $b$*

Model B's surrogate objective uses an exponent $b \in (0, 1)$ in $F_B(T) = \sum_{(i,j)\in A} L_{ij}^{w}|Q_{ij}|^{b}$ to represent economies of scale in pipeline cost. To illustrate the directional effect of this modelling choice, we report one Scenario 2 run at $b = 0.4$ and one at $b = 0.8$ alongside the replicated baseline results at $b = 0.6$ (Table 2). The additional cases are descriptive only and are not used to characterise stochastic sensitivity or identify an optimal exponent.

Table 2: Scenario 2: indicative sensitivity of Model B to the flow-cost exponent $b$. Values for $b = 0.4$ and $b = 0.8$ are from single runs; $b = 0.6$ is reported as mean±SD over five runs.

| **Metric** | $b = 0.4$ **(1 run)** | $b = 0.6$ **(mean±SD)** | $b = 0.8$ **(1 run)** |
|---|---|---|---|
| Total length (km) | 279.0 | $294.3 \pm 4.2$ | 311.1 |
| Total CAPEX (£M) | 667.6 | $587.4 \pm 7.0$ | 760.8 |
| Cost per km (£M/km) | 2.39 | $2.00 \pm 0.02$ | 2.45 |
| Trunk length share (%) | 33.6 | 29.1 | 27.8 |
| Trunk cost share (%) | 39.7 | 41.6 | 32.6 |

For $b = 0.4$, the objective is closer to pure length minimisation; the total network is relatively short (279 km) but CAPEX remains high (667.6 £M), with a long backbone carrying a large share of flow (trunk length and cost shares of 33.6% and 39.7%). Increasing $b$ to 0.6 strengthens the penalty on high-flow segments: the model accepts extra network length and slightly higher trunk cost share (41.6%), but shortens and repositions the backbone and, in the cases reported here, is associated with the lowest CAPEX of the three illustrated exponent values (587.4 £M, $\approx 2.00$ £M/km). Pushing $b$ further to 0.8 makes the optimisation strongly averse to heavily loaded segments. The

model responds by diffusing flows over a longer, more ramified network (311.1 km), reducing the trunk's share of system cost to 32.6% but increasing both total CAPEX (760.8 £M) and cost per kilometre (2.45 £M/km).

These illustrative cases are consistent with a possible interior trade-off between backbone shortening and excessive flow spreading. However, because the $b = 0.4$ and $b = 0.8$ cases are single runs and no replicated parameter sweep or calibration was performed, these results do not establish $b = 0.6$ as optimal or identify a preferred exponent.

### *4.4. Impact of spatial redistribution of flows (Scenario 3)*

Scenario 3 repeats Scenario 2 but increases capture at the peripheral West Burton source. Figure 5 shows the resulting Model B network; the Scenario 2 layout is shown in Figure 4. The main corridor is pulled southwards into a U-shape, running closer to the more highly emitting node — West Burton. The pink arrows in Figure 5 indicate the sections where the trunk shifts relative to Scenario 2. Model A's topology does not change between Scenarios 2 and 3 because its Stage 1 objective depends only on terminal locations and the penalty surface, not on flow magnitudes. However, Stage 2 sizing and cost outcomes still change because design flows change. We therefore omit the Model A map comparison here and focus on the trunk shift exhibited by Model B.




Figure 5: Scenario 3 (peripheral intensification): Model B network after increasing capture at West Burton; arrows indicate where the trunk shifts relative to Scenario 2.

Table 3 summarises the system response under Model B. Increasing West Burton raises total captured $CO_2$ by 36%, while total network length increases by 11% and total CAPEX by 26%. The key effect is a reallocation towards the backbone: trunk length share increases modestly (29.1% to 33.0%), but trunk CAPEX share rises sharply (41.6% to

51.7%). Consistent with the map-level trunk shift, 91.1% of the incremental investment from Scenario 2 to Scenario 3 is absorbed by trunk segments.

Table 3: Scenario 3 response under Model B relative to the Scenario 2 mean (Scenario 2 mean from five runs; Scenario 3 is a single illustrative run). The trunk is defined as the Easington–Drax path on the tree.

| **Headline metric** | **Scenario 2 (mean)** | **Scenario 3** | **Change** |
|---|---|---|---|
| Total captured $CO_2$ ($MtCO_2$/yr) | 28.15 | 38.36 | +36.3% |
| Total network length (km) | 294.34 | 326.60 | +11.0% |
| Total network CAPEX (£M) | 587.36 | 739.10 | +25.8% |
| Trunk length share (%) | 29.08 | 33.05 | +4.0 pp |
| Trunk CAPEX share (%) | 41.56 | 51.72 | +10.2 pp |
| Share of incremental CAPEX on trunk (%) | – | 91.1 | – |

This indicates that the economically optimal design is highly sensitive to large peripheral emitters: rather than simply adding local branches, the model reinforces and repositions shared backbone infrastructure to accommodate the new flow centre. In practical terms, a single high-volume site can materially reshape the trunk corridor and concentrate additional spending on shared assets, whereas distance-based routing (Model A) cannot express this behaviour because the topology is invariant to flow redistribution.

### *4.5. Cross-scenario discussion and implications*

Across scenarios, the key finding is structural: once pipeline costs depend on flow through discrete diameter choices and non-linear economies of scale, the optimisation is driven less by total network extent and more by the placement and length of the high-flow backbone. Penalised detours that are attractive under length-based routing can become economically dominated if they elongate the trunk, because a relatively small increase in trunk length can push many kilometres of pipe into larger diameter classes.

**Q1 (comparison):** In Scenario 1, Model B yields networks that overlap more closely with the published HCCP network than Model A under the buffer-overlap metric. Because neither model uses the published alignment as an input, this indicates that internalising flow-dependence in Stage 1 systematically biases routing towards trunk placements more consistent with an engineered design.

**Q2 (system design):** In Scenario 2, Model B is longer and more penalty-exposed on average, yet it is substantially cheaper once evaluated by the common Stage 2 sizing model. The qualitative mechanism is consistent across runs: Model A reduces penalty-weighted length partly by detouring the backbone around high-penalty terrain, which can inadvertently create a long high-capacity trunk (here, the Easington–Drax path) that accumulates large-diameter cost

over many kilometres. Model B accepts selected penalty exposure to keep the trunk shorter and redistributes connectivity into additional lower-flow spurs; under flow-dependent costs, this trunk-shortening effect dominates total CAPEX.

**Illustrative $b$ variation:** The single-run cases at $b = 0.4$ and $b = 0.8$ illustrate the expected directional trade-off: lower $b$ places greater emphasis on network length, while higher $b$ more strongly discourages highly loaded segments and can diffuse flow over a longer network. These cases are descriptive and are not used to select or optimise the baseline exponent.

**Q3 (spatial sensitivity):** In Scenario 3, increasing a single peripheral emitter is sufficient to re-centre the economically optimal backbone and to concentrate most incremental investment on trunk segments. Model A's routing/topology is invariant to flow magnitudes, but its sized diameters and costs still change in Stage 2; the distinctive effect is that only the flow-dependent routing objective can express a corridor shift of the trunk in response to spatial redistribution of emissions.

## 5. Conclusions

This paper tested how CCS transport network designs change when flow-dependent pipeline economics are internalised in the routing objective. We proposed a two-stage framework in which Stage 1 generates geography-aware tree topologies on a raster penalty surface, and Stage 2 sizes and costs every candidate layout using the same hydraulic and discrete-diameter optimisation model. Because Stage 2 is held fixed, differences in cost and sizing outcomes isolate the effect of the routing objective.

Three findings follow. First, in the corridor-comparison case (Scenario 1), the flow-aware layouts have greater buffer overlap with the published HCCP corridor than the penalty-weighted-length layouts. This provides an external plausibility comparison but, given the unmodelled determinants of the engineered route, is not interpreted as causal validation of the flow-dependence hypothesis. Second, in the full regional build-out (Scenario 2), the best-found layouts generated by the flow-aware surrogate are slightly longer ($\sim 6\%$ in geometric length) but have substantially lower estimated CAPEX ($\sim 35\%$, from $\sim$ 906M to $\sim$ 587M) than those generated by the penalty-weighted-length objective when both are evaluated using the same Stage 2 model. Within this comparison, trunk placement and length have a greater influence on CAPEX than total route length or mean penalty exposure. Third, when a peripheral site's emission is increased (Scenario 3), the economically optimal backbone re-centres and absorbs the majority of incremental investment (order-$90\%$ on trunk segments), whereas the minimum-length model cannot express such a corridor shift because its Stage 1 topology is invariant to flow magnitudes.

The practical message from this comparison is that trunk alignment should be considered explicitly in CCS net-

work planning, rather than emerging only as a consequence of penalty-weighted-length minimisation. Within the adopted framework, the penalty-weighted-length heuristic generates geographically plausible layouts that incur substantially higher estimated CAPEX after detailed diameter selection than those generated by the flow-aware surrogate. Introducing flow dependence into Stage 1 therefore provides a practical means of exploring alternative backbone placements while retaining consistent engineering evaluation through the common Stage 2 model.

Several modelling choices bound what can be inferred from the absolute numbers: designs are restricted to loop-free trees (no redundancy), sized for steady design flows, and evaluated with correlation-based CAPEX and simplified hydraulics under representative $CO_2$ properties. The raster penalty surface remains a proxy for constructability/consentability rather than an explicit permitting or construction process. These assumptions are applied identically across routing models, so the relative differences reported here are attributable to internalising flow-dependence in the routing objective within this framework.

A key direction for further work is multi-period investment timing under uncertainty, with trunk placement treated as a least-regret decision: designing backbones that remain near-optimal across uncertain capture deployment, phasing, and spatial shifts in emissions. This naturally motivates robust or stochastic extensions (e.g. minimax regret over scenarios, or distributionally-robust formulations) that preserve tractability while explicitly valuing flexibility in trunk siting and staged capacity expansion.

## CRediT author statement

**Joseph Hammond**: Conceptualisation, Data Curation, Methodology, Investigation, Analysis, Visualisation, Supervision, Writing - Original Draft, Writing - Review & Editing.

**Joel Thornton**: Writing - Original Draft, Writing - Review & Editing.

**Solomon Brown**: Supervision, Writing - Review & Editing.

## Funding sources

This research did not receive any specific grant from funding agencies in the public, commercial, or not-for-profit sectors.

## Declaration of competing interest

The authors declare that they have no known competing financial interests or personal relationships that could have appeared to influence the work reported in this paper.

## Generative AI statement

During the preparation of this manuscript, the authors used generative AI tools to assist with drafting and editing text for clarity and readability. All AI-assisted content was reviewed and edited by the authors, who take full responsibility for the final manuscript.

## Appendix A. Genetic algorithm settings

Table A.4 summarises the genetic algorithm (GA) parameters used for all Stage 1 routing runs. Unless stated otherwise, identical settings are used for Model A and Model B to ensure differences in outcomes are attributable to the objective function rather than to search configuration.

Table A.4: Stage 1 GA parameters used for routing optimisation.

| **Parameter** | **Value** | **Notes** |
|---|---|---|
| Population size | 1000 | Number of candidate genomes per generation. |
| Tournament size | 2 | Tournament selection pressure (binary tournament). |
| Est. number of generations | 1500 | Estimated number of generations (used to calibrate feasible-mutation probability across generations) |
| Convergence window | 150 | Number of generations over which improvement is assessed. |
| Convergence threshold | 0.01 | Terminate if best-objective change over the convergence window is below this threshold (relative). |
| Feasible-mutation probability (min) | 0.60 | Lower bound for probability of feasible mutation operator. |
| Feasible-mutation probability (max) | 0.99 | Upper bound for probability of feasible mutation operator. |
| Random seed | 42 | Default seed; runs use distinct seeds as required for replication. |

## Appendix B. Penalty surface feature weights and sources

Table B.5 lists the GIS feature layers used to construct the raster penalty surface and the corresponding penalty multipliers. A multiplier of 1 denotes unconstrained terrain. Higher values represent greater relative routing difficulty/undesirability and are intended as a proxy for combined constructability, permitting and consentability effects. Vector layers are rasterised to the routing grid and combined to form a composite cell multiplier $\phi_g \geq 1$ used in

Eq. (2). Overlapping layers combine additively in excess over baseline according to Eq. (1), so that $\phi_g = 1$ denotes unconstrained terrain and $\phi_g = w_f$ when only a single feature layer $f$ is present.

Table B.5: Penalty weights and data sources for cost-surface features.

| **Feature** | **Penalty multiplier** | **Source** |
|---|---|---|
| SPA/SAC | 30 | [18] |
| Ramsar | 10 | [18] |
| SSSI | 10 | [19] |
| Ancient woodland | 14 | [20] |
| Woodland | 7 | [21] |
| Peaty soils / deep peat | 1.6 | [19] |
| Surface water area | 5 | [21] |
| Tidal water | 10 | [21] |
| Foreshore (coastal) | 2.7 | [21] |
| National parks | 7 | [20] |
| AONB | 30 | [19] |
| Conservation areas | 20 | [22] |
| Parks & gardens (registered) | 5 | [20] |
| Scheduled monuments | 30 | [22] |
| Buildings | 30 | [21] |
| Major road network | 1.9 | [21] |
| Railways | 2.2 | [21] |
| CRoW access land | 20 | [19] |

The penalty multipliers were specified a priori based on the relative geographical cost weightings reported by Van Den Broek et al. [23] and previously applied within StObGA by Hammond et al. [13]. They were not calibrated against the results of the present study. They represent relative traversal penalties rather than site-specific construction-cost estimates.

## Appendix C. Stage 2 sizing model (summary and parameters)

Stage 2 sizes each candidate tree on a fixed topology with fixed design flows $Q_{ij}$ and geometric lengths $L_{ij}$. $CO_2$ is modelled as a single-phase dense-phase fluid with constant representative properties and design limits (Table C.6).

For each arc $(i, j) \in A$, the optimisation selects (i) the number of parallel pipelines $N_{ij}^{p}$ and (ii) one discrete diameter–schedule option from a commercial catalogue, and determines nodal pressures such that hydraulic, operational, and structural constraints are satisfied. The Stage 2 objective is to minimise total network CAPEX (as defined in the main text).

The model is implemented in Pyomo and solved using BARON. Global optimality is sought, and only solutions reported by BARON as globally optimal are retained; locally optimal solutions are not accepted. For the fixed-topology networks considered here, Stage 2 solution times typically range from approximately 0.8 to 10 s per network. Further details of the sizing model and its implementation are provided in [7] and [13].

*Discrete diameter selection and parallel lines*

Let $\mathcal{D}$ index the commercial diameter–schedule catalogue, where each option $d \in \mathcal{D}$ defines an inner/outer diameter pair $(D_d^{pi}, D_d^{po})$ and wall thickness $t_d$. Binary variables $B_{ijd} \in \{0, 1\}$ select exactly one catalogue option per arc:

$$\sum_{d \in \mathcal{D}} B_{ijd} = 1, \qquad \forall (i, j) \in A. \tag{C.1}$$

Selected pipe dimensions are

$$D_{ij}^{pi} = \sum_{d \in \mathcal{D}} D_d^{pi}\, B_{ijd}, \quad D_{ij}^{po} = \sum_{d \in \mathcal{D}} D_d^{po}\, B_{ijd}, \quad t_{ij} = \sum_{d \in \mathcal{D}} t_d\, B_{ijd}, \tag{C.2}$$

with $D_{ij}^{po} = D_{ij}^{pi} + 2t_{ij}$.

If an arc is implemented using $N_{ij}^{p}$ identical parallel pipelines, the arc flow is split equally:

$$Q_{ij}^{p} = \frac{Q_{ij}}{N_{ij}^{p}}, \qquad \forall (i, j) \in A. \tag{C.3}$$

*Hydraulic and operational constraints*

Let $P_i$ denote nodal pressure and $\Delta P_{ij} = P_i - P_j$ the pressure drop on arc $(i, j)$. Nodal pressures are bounded:

$$P^{\min} \le P_i \le P^{\max}, \qquad \forall i \in N, \tag{C.4}$$

where $P^{\min}$ and $P^{\max}$ are given in Table C.6.

Hydraulic feasibility is enforced using a Darcy–Weisbach-based sizing relation with constant representative dense-phase properties. Let $\dot{V}_{ij}^{p}$ denote the per-pipeline volumetric flow rate ($m^3$/s), obtained by converting the per-pipeline

mass flow $Q^p_{ij}$ ($MtCO_2$/yr) to kg/s and dividing by the assumed constant density $\rho$ (Table C.6). The required inner diameter to carry $\dot{V}^p_{ij}$ over length $L_{ij}$ under pressure gradient $\Delta P_{ij}/L_{ij}$ is:

$$D^{pi}_{ij} \geq \left( \frac{8 f_D \rho (\dot{V}^p_{ij})^2}{\pi^2 \left( \frac{\Delta P_{ij}}{L_{ij}} \right)} \right)^{1/5}, \qquad \forall (i,j) \in A, \tag{C.5}$$

where $f_D$ is the (constant) Darcy friction factor from Table C.6.

Per-pipeline average velocity on arc $(i,j)$ is:

$$v_{ij} = \frac{4\dot{V}^p_{ij}}{\pi (D^{pi}_{ij})^2}, \qquad \forall (i,j) \in A. \tag{C.6}$$

To limit internal wall shear (used here as a conservative proxy for erosion/attrition risk), we impose a shear-based maximum velocity. Using the Darcy wall-shear relationship $\tau_{w,ij} = (f_D/8)\rho v^2_{ij}$, the corresponding shear-limited velocity is:

$$v^e = \sqrt{\frac{8\,\tau^w}{\rho\, f_D}}, \tag{C.7}$$

and the operational constraint is:

$$v_{ij} \leq v^e, \qquad \forall (i,j) \in A, \tag{C.8}$$

where $\tau^w$ is an assumed allowable wall shear stress.

*Structural constraint*

Minimum wall thickness is enforced using the hoop-stress relationship:

$$t_{ij} \geq \frac{P^{\mathrm{MOP}}\, D^{po}_{ij}}{2\,\tau^p\, \kappa^E\, \kappa^{DF}}, \qquad \forall (i,j) \in A, \tag{C.9}$$

where $P^{\mathrm{MOP}}$, $\tau^p$, $\kappa^{DF}$, and $\kappa^E$ are given in Table C.6.

*$CO_2$ properties and design limits*

Table C.6: Assumed dense-phase $CO_2$ properties and design limits used in Stage 2 (constant representative values).

| **Parameter** | **Value** | **Notes / units** |
|---|---|---|
| Molar mass | 44.01 | g/mol |
| Specific heat ratio | 1.28 | – |
| Temperature | 301.15 | K (28 °C) |
| Density, $\rho$ | 735.0 | kg/m$^3$ (representative dense-phase value) |
| Dynamic viscosity, $\mu$ | $6.06 \times 10^{-5}$ | Pa·s |
| Friction factor, $f_D$ | 0.013 | constant |
| Pipe roughness, $\xi$ | $4.57 \times 10^{-5}$ | m (carbon steel) |
| Min node pressure, $P^{\min}$ | $8.5 \times 10^6$ | Pa |
| Max node pressure, $P^{\max}$ | $12.5 \times 10^6$ | Pa |
| Default sink pressure | $11.0 \times 10^6$ | Pa |
| Max operating pressure, $P^{\mathrm{MOP}}$ | $12.5 \times 10^6$ | Pa |
| SMYS, $\tau^p$ | $414 \times 10^6$ | Pa (X60) |
| Design factor, $\kappa^{DF}$ | 0.72 | – |
| Joint factor, $\kappa^E$ | 1.0 | – |

These assumptions are applied identically to layouts from Model A and Model B.

## Appendix D. Costing assumptions and UK uplift factors

This appendix summarises how the pipeline CAPEX correlations used in Stage 2 are constructed and expressed on the study cost basis (May 2025 GBP). The objective is not to create a project-grade estimate, but to (i) retain the widely used economies-of-scale behaviour in [15] and (ii) apply a transparent, documented set of escalations and UK-specific uplifts so that Model A and Model B layouts are costed consistently.

*A. Base CAPEX model and study cost basis (May 2025 GBP)*

Stage 2 segment CAPEX is computed using the four McCoy–Rubin cost blocks (materials, labour, right-of-way, and miscellaneous/indirects) as a function of outside diameter $D_{ij}$ and geometric length $L_{ij}$. As stated in Section 2, the coefficients used in Eq. (10) are already expressed on the study cost basis (May 2025 GBP), i.e. after:

(i) escalation using the Chemical Engineering Plant Cost Index (CEPCI; 444.2 $\rightarrow$ 800; combined factor applied in this study: 1.80),

(ii) conversion to GBP using a May 2025 USD–GBP exchange-rate assumption, and

(iii) multiplication by UK block-specific modifiers (below) to reflect systematic UK–US construction uplifts by cost block.

These adjustments are applied at the cost-block level (materials/labour/ROW/misc), not as a single post-hoc multiplier, to preserve the relative composition of CAPEX with diameter.

*B. UK block-specific uplift factors*

Table D.7 documents the UK uplift multipliers applied to each CAPEX block to convert the McCoy–Rubin US cost basis to an indicative UK basis. These multipliers are intended to capture broad, persistent differences (e.g. steel price levels, labour costs, land values, professional/regulatory overheads), rather than local micro-routing effects, which are handled separately via the route penalty factor $\bar{\phi}_{ij}$ (Eq. (9)).

Table D.7: UK uplift factors applied by CAPEX cost block (study basis: May 2025 GBP).

| **Cost block** | **UK uplift** | **Basis (data series / evidence)** |
|---|---|---|
| Materials (steel) | $\times 1.20$ | Indicative UK mill-gate steel price level $\sim$20% above US on a rebased index comparison using ONS steel series and US producer price indices. [24, 25] |
| Site labour & plant | $\times 1.35$ | Relative construction earnings/indices suggest UK labour costs above US, partially offset by productivity differences for mainline spread work; net uplift applied as $\sim$35%. [26, 27] |
| Right-of-way / land | $\times 1.30$ | UK agricultural land values materially above US on headline price-per-acre comparisons; effective ROW uplift moderated to reflect mixed rural/peri-urban routing and partial land-take. [28, 29] |
| Miscellaneous / indirects | $\times 1.70$ | Higher UK professional services, permitting, and regulatory overheads (fees, legal/consultancy rates, project overheads) relative to US benchmarks; net uplift taken as $\sim$70%. [30–35] |

*C. Interaction with the spatial penalty surface*

Local, route-dependent construction difficulty/undesirability is represented separately from the UK–US uplift factors. For each segment $(i, j)$, the raster penalty surface induces a mean penalty factor $\bar{\phi}_{ij} \geq 1$ (Eq. (9)), which is applied multiplicatively to the segment CAPEX in Eq. (10). This ensures that:

(i) the routing objective in Stage 1 and the CAPEX uplift in Stage 2 are consistent (both derived from the same raster), and

(ii) UK-wide uplifts (Table D.7) are not conflated with local corridor effects (captured by $\bar{\phi}_{ij}$).

*D. Reasonableness check against public HyNet cost information*

As a reasonableness check, the resulting May 2025 GBP cost model was compared against the limited publicly-available cost information for the HyNet $CO_2$ pipeline. This check is used only to confirm that implied costs are in the correct order of magnitude for UK trunk pipelines under comparable length/diameter assumptions; it is not treated as a calibration target, and the coefficients in Eq. (10) are not tuned to match HyNet.

## References


[1] M. Reuß, L. Welder, J. Thürauf, J. Linßen, T. Grube, L. Schewe, D. Stolten, M. Robinius, Modeling hydrogen networks for future energy systems: A comparison of linear and nonlinear approaches, International Journal of Hydrogen Energy 44 (60) (2019) 32136–32150. doi:10.1016/j.ijhydene.2019.10.080.

[2] M. Moreno-Benito, P. Agnolucci, L. G. Papageorgiou, Towards a sustainable hydrogen economy: Optimisation-based framework for hydrogen infrastructure development, Computers & Chemical Engineering 102 (2017) 110–127. doi:10.1016/j.compchemeng.2016.08.005.

[3] F. Parolin, P. Colbertaldo, S. Campanari, Benefits of the multi-modality formulation in hydrogen supply chain modelling, E3S Web of Conferences 334 (2022) 02003. doi:10.1051/e3sconf/202233402003.
URL https://www.e3s-conferences.org/articles/e3sconf/abs/2022/01/e3sconf_efc2022_02003/e3sconf_efc2022_02003.html

[4] L. Welder, D. S. Ryberg, L. Kotzur, T. Grube, M. Robinius, D. Stolten, Spatio-temporal optimization of a future energy system for power-to-hydrogen applications in germany, Energy 158 (2018) 1130–1149. doi:10.1016/j.energy.2018.05.059.

[5] S. Baufumé, F. Grüger, T. Grube, D. Krieg, J. Linßen, M. Weber, J. Hake, D. Stolten, Gis-based scenario calculations for a nationwide german hydrogen pipeline infrastructure, International Journal of Hydrogen Energy 38 (10) (2013) 3813–3829. doi:10.1016/j.ijhydene.2012.12.147.

[6] A. C. Weber, L. G. Papageorgiou, Design of hydrogen transmission pipeline networks with hydraulics, Chemical Engineering Research and Design 131 (2018) 266–278. doi:10.1016/j.cherd.2018.01.022.

[7] J. O. Ejeh, S. B. Martynov, S. F. Brown, An minlp model for the optimal design of $co_2$ transportation infrastructure in industrial clusters, in: Computer Aided Chemical Engineering: 33rd European Symposium on Computer Aided Process Engineering (ESCAPE-33), Vol. 52 of Computer Aided Chemical Engineering, Elsevier, Amsterdam, 2023, pp. 3085–3090. doi:10.1016/B978-0-443-15274-0.50492-3.

[8] T. L. Magnanti, R. T. Wong, Network design and transportation planning: Models and algorithms, Transportation Science 18 (1) (1984) 1–55. doi:10.1287/trsc.18.1.1.

[9] P. W. Heijnen, E. J. Chappin, P. M. Herder, A method for designing minimum-cost multisource multisink network layouts, Systems Engineering 23 (1) (2019) 14–35. doi:10.1002/sys.21492.

[10] J. André, S. Auray, J. Brac, D. D. Wolf, G. Maisonnier, M.-M. Ould-Sidi, A. Simonnet, Design and dimensioning of hydrogen transmission pipeline networks, European Journal of Operational Research 229 (1) (2013) 239–251. doi:10.1016/j.ejor.2013.02.036.

[11] C. Yeates, C. Schmidt-Hattenberger, W. Weinzierl, D. Bruhn, Heuristic methods for minimum-cost pipeline network design: A node valency transfer metaheuristic, Networks and Spatial Economics 21 (2021) 839–871. doi:10.1007/s11067-021-09550-9.

[12] R. S. Middleton, S. P. Yaw, B. A. Hoover, K. M. Ellett, Simccs: An open-source tool for optimising $co_2$ capture, transport, and storage infrastructure, Environmental Modelling & Software 124 (2020) 104560. doi:10.1016/j.envsoft.2019.104560.

[13] J. Hammond, M. Rosenberg, S. Brown, Understanding costs in hydrogen infrastructure networks: A multi-stage approach for spatially-aware pipeline design, International Journal of Hydrogen Energy 102 (2025) 430–443. doi:10.1016/j.ijhydene.2024.12.273.

[14] M. Rosenberg, T. French, M. Reynolds, L. While, A genetic algorithm approach for the euclidean steiner tree problem with soft obstacles, in: F. Chicano, K. Krawiec (Eds.), GECCO '21: Proceedings of the Genetic and Evolutionary Computation Conference, Association for Computing Machinery (ACM), USA, 2021, pp. 618–626. doi:10.1145/3449639.3459397.

[15] S. T. McCoy, E. S. Rubin, An engineering-economic model of pipeline transport of $CO_2$ with application to carbon capture and storage, International Journal of Greenhouse Gas Control 2 (2) (2008) 219–229. doi:10.1016/S1750-5836(07)00119-3.
URL https://doi.org/10.1016/S1750-5836(07)00119-3

[16] Net Zero North Sea Storage Limited, Humber carbon capture pipeline: Programme document, document Ref: 10607856-ARC-XX-XX-XX-TC-0001-P1, Revision V4 (Feb. 2025).
URL https://nephccp.co.uk/assets/images/pdf/Programme_Document10607856-ARC-XX-XX-XX-TC-0001-P1_V.4.pdf

[17] Department for Energy Security and Net Zero, Department for Environment, Food and Rural Affairs, Uk national atmospheric emissions inventory (naei): Uk emissions dataset (2024 publication), accessed via the NAEI UK emissions data selector; licensed under the Open Government Licence v3.0. (2024).
URL https://naei.energysecurity.gov.uk/data/data-selector

[18] Joint Nature Conservation Committee (JNCC), Uk protected area datasets for download (05 2025).
URL https://jncc.gov.uk/our-work/uk-protected-area-datasets-for-download/

[19] Natural England, Natural england open data geoportal.
URL https://naturalengland-defra.opendata.arcgis.com/

[20] UK Government, Find open data  data.gov.uk.
URL https://www.data.gov.uk/

[21] Ordnance Survey, Os openmap–local.
URL https://www.ordnancesurvey.co.uk/products/os-open-map-local

[22] Historic England, National heritage list for england (nhle): Data downloads.
URL https://historicengland.org.uk/listing/the-list/data-downloads/

[23] M. van den Broek, P. Mesquita, J. Carneiro, J. R. Silva, N. Berghout, A. Ramírez, J. P. Gouveia, J. Seixas, H. Cabal, R. Martinez, A. Rimi, Y. Zarhloule, M. Sardinha, D. Boavida, G. Tosato, Region specific challenges of a co2 pipeline infrastructure in the west mediterranean sea, Energy Procedia 37 (2013) 3137–3146. doi:10.1016/j.egypro.2013.06.200.

[24] Office for National Statistics, Ppi index output domestic - c2410 basic iron and steel and ferro-alloys 2015=100 (series id: Ew6t), source dataset: Producer price inflation time series (MM22) (Feb. 2025).
URL https://www.ons.gov.uk/economy/inflationandpriceindices/timeseries/ew6t/mm22

[25] U.S. Bureau of Labor Statistics, Producer price index by commodity: Metals and metal products: Steel mill products (wpu1017), original

source: BLS Producer Price Index (2025).

URL https://fred.stlouisfed.org/series/WPU1017

[26] Office for National Statistics, Average weekly earnings: Construction (total pay excluding arrears), seasonally adjusted (series id: K553), oNS time series dataset: EMP (Jun. 2024).

URL https://www.ons.gov.uk/economy/grossdomesticproductgdp/timeseries/k553/emp/previous/v103

[27] U.S. Bureau of Labor Statistics, Table b-3. average hourly and weekly earnings of all employees on private nonfarm payrolls by industry sector, seasonally adjusted (2025).

URL https://www.bls.gov/news.release/empsit.t19.htm

[28] Savills Research, Gb farmland market in minutes uk rural (summer 2024) (2024).

URL https://pdf.savills.com/documents/GB-Farmland-Market-in-Minutes-Summer-24.pdf

[29] U.S. Department of Agriculture, National Agricultural Statistics Service, Land values 2024 summary (Aug. 2024).

URL https://www.nass.usda.gov/Publications/Todays_Reports/reports/land0824.pdf

[30] Environment Agency, Environmental permits: when and how you are charged, guidance (GOV.UK) (Sep. 2025).

URL https://www.gov.uk/government/publications/environmental-permitting-charges-guidance/environmental-permitting-charges-guidance

[31] Environment Agency, Environmental permits and abstraction licences: tables of charges, charging tables (GOV.UK) (2025).

URL https://www.gov.uk/government/publications/environmental-permits-and-abstraction-licences-tables-of-charges

[32] PwC, Law firm performance surpasses expectations with continued growth amidst global market volatility pwc law firms' survey 2024 (Oct. 2024).

URL https://www.pwc.co.uk/press-room/press-releases/research-commentary/2024/law-firm-performance-surpasses-expectations-with-continued-growt.html

[33] Financial Times, Top uk law firms raise hourly rates by 40% in five years, article (subscription may be required) (Oct. 2024).

URL https://www.ft.com/content/541f8b38-d657-4542-a7de-8c92a113db28

[34] LawPay, How much is a lawyer? hourly rates by state and more in 2023 (Sep. 2025).

URL https://www.lawpay.com/about/blog/lawyer-hourly-rate-by-state/

[35] Federal Energy Regulatory Commission, Filing fees (Mar. 2025).

URL https://www.ferc.gov/filing-fees